Phase-sensitive transport at a normal metal–superconductor interface close to a Josephson junction

David Gosselin, Gaston Hornecker, Régis Mélin, and Denis Feinberg*
Université Grenoble-Alpes, Institut NEEL, F-38042 Grenoble Cedex 9, France
and CNRS, Institut NEEL, F-38042 Grenoble Cedex 9, France
(Received 25 October 2013; revised manuscript received 24 December 2013; published 14 February 2014)

Phase- and voltage bias-sensitive quasiparticle transport at a double NIS_1IS_2 interface is considered. The barriers I range from tunnel to transparent, and the intermediate region S_1 has a width comparable to the superconducting coherence length. A phase difference φ is applied to the Josephson junction S_1IS_2. The normal and Andreev reflections at the NIS_1 interface become φ sensitive, and transport is governed by interferences within the narrow S_1 region in both the normal and the anomalous channels. The subgap conductance is separately (energy E) and (phase φ) symmetric. Above the superconducting gap, the conductance is, in general, not symmetric even if (E,φ) is changed in $(-E,-\varphi)$, but the symmetry is restored by averaging Fermi oscillations. The Tomasch oscillations are amplified by the phase difference. The subgap conductance exhibits a resonant structure at the energy of the Andreev bound states (ABSs) of the S_1IS_2 junction, providing a side spectroscopy of such states. Depending on the relative transparencies of the junctions, the resonance can increase or reduce the conductance, and it can even vanish for $\varphi = \pi$, featuring total reflection of quasiparticles at NS_1 by the ABS at S_1S_2.

DOI: 10.1103/PhysRevB.89.075415 PACS number(s): 74.78.Na, 74.45.+c

I. INTRODUCTION

Transport in hybrid setups involving interfaces between superconductors (S) and normal metals (N) is governed by Andreev reflection, where an incoming electron with energy $\mu + E$ is transformed into a hole with opposite energy $\mu - E$ in the metal (μ is the chemical potential) [1,2] and a Cooper pair enters the superconducting condensate. Conversely, an incoming hole may be reflected as an electron while a pair is taken from S. Andreev scattering dominates subgap transport and it also plays a role at energies on the order of a few times the superconducting gap. Using the Bogoliubov-De Gennes equations and writing the scattering equations for the electron and hole wave functions, De Gennes and Saint-James found subgap bound states in a thin metallic layer in contact with a superconductor [2]. Rowell and McMillan [3] showed that conductance oscillations occur as well above the gap. Tomasch [4] discovered oscillations in the conductance above the gap in a $NSIN$ structure, which were explained by McMillan and Anderson [5] as an interference effect due to the wave-vector mismatch between the electron and holelike quasiparticle branches propagating in a narrow S layer of thickness L on the order of the superconducting coherence length ξ.

Using the scattering approach, Blonder, Tinkham, and Klapwijk [6] were able to bridge the gap between a Giaever tunneling barrier (NIS) and a perfectly transparent NS interface, where the conductance is doubled below the gap, with respect to the normal case. The scattering approach had been used previously for a double SNS interface by Kulik [7] in the transparent case, then in many subsequent works, to obtain a complete description of a clean $SINIS$ Josephson junction. It is characterized by the formation of Andreev bound states (ABSs), as resonant states formed by multiple electron-electron and electron-hole scattering at each SIN interface. The phase dispersion of the ABS is responsible for the Josephson current flowing through the junction. Recently, a tunnel spectroscopy of the ABS was performed by attaching a third contact to the normal bridge of a long junction [8]. A microwave spectroscopy of the ABS was recently obtained in an atomic point contact [9,10] and a diffusive metallic junction [11].

These effects have been probed experimentally in two-terminal transport geometries. In addition, tunnel spectroscopy of the ABS involves a third reservoir, weakly coupled directly to the junction [8,12]. Coupling a SNS Josephson junction to a normal wire has also been proposed and achieved [13]. Recently, new three-terminal hybrid configurations exploiting the mesoscopic size of Cooper pairs have been explored. For instance, consider a $NISIN$ geometry where two normal leads (or quantum dots) are connected by a narrow superconducting region of size comparable to the superconducting coherence length ξ. Then a mechanism denoted as crossed (or nonlocal) Andreev reflection allows a hole incoming on one side to be transmitted as an electron on the other, effectively splitting a Cooper pair from the superconductor into a pair of correlated quasiparticles [14]. Those carry opposite energies and spins (for an s-wave superconductor), and this mechanism has been proposed as a source of entangled fermions in the solid state [15]. A three-terminal all-superconducting $SISIS$ setup, called a Josephson bijunction, has been more recently considered [16–21]. It was shown that the two independent phase degrees of freedom (or voltages) lead to coherent multipair dc channels which coexist with dissipative quasiparticle transport for some combinations of applied voltages.

In what follows, we investigate a hybrid structure where Andreev reflection interferes with Josephson transport at a neighboring junction. It is controlled by one voltage and one phase as *independent* variables. More specifically, we explore the properties of a hybrid bijunction NIS_1IS_2, made of a NIS_1 interface, in close proximity with a Josephson junction S_1IS_2. The transparencies of the two interfaces are arbitrary. The Josephson junction is biased with a phase difference φ. A possible experimental device is sketched on Fig. 1. Alternatively, the phase difference can also be imposed by

*denis.feinberg@neel.cnrs.fr

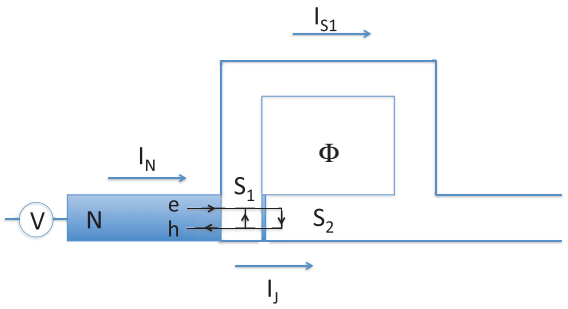

FIG. 1. (Color online) Schematics of a hybrid NS loop setup. A superconducting loop at zero voltage, cut by a Josephson junction, is connected on the left to a normal metal lead, at a voltage V, at a distance from the junction comparable to the coherence length (in practice, the loop thickness is larger than pictured). The flux Φ imposes a phase difference φ at the junction. The total current I_N splits into a Josephson current I_J and a current I_{S1} flowing in the upper branch of the loop. The scattering model is one-dimensional and involves a double NS_1S_2 interface, where S_1 and S_2 are the parts of the (same) superconductor, set at phases 0 and φ by convention. The incident electron and scattered hole waves are represented, together with Andreev reflection processes within S_1 and those within S_2, close to the junction that generates the ABSs.

an applied current, in a three-terminal geometry, but accessing only the range $\varphi = [-\pi/2,\pi/2]$.

To modelize such a structure, we consider a one-dimensional scattering model with two interfaces in series. As a consequence, the currents at the interfaces NIS_1 et S_1IS_2 are not necessarily equal. The quasiparticle current in N is converted into a Cooper pair current flowing partly through the junction and partly in the upper branch of the loop. In spite of the presence of interferences in this setup, the geometry is very different from the usual Andreev interferometer containing two NS interfaces in parallel [22]. The conductance through the NIS_1 interface is calculated within the scattering approach. The phase difference between S_1 and S_2, as a new control variable, brings quantitative and qualitative changes as compared to previous calculations including scattering within a single superconductor [23]. Resonant tunneling in a $NSNSN$ double barrier geometry was also investigated in Ref. [24], focusing on the case of ideal NS interfaces. Conversely, we consider here an asymmetric NS_1S_2 structure where, in addition, the transparencies of the NS_1 and S_1S_2 junctions are arbitrary.

In this work, we calculate the conductance $G(E,\varphi)$ as a function of the voltage energy $E = \mathrm{eV}$ and the phase φ. This conductance is the derivative of the current through the NIS_1 interface with respect to the voltage V on N, the two superconducting regions S_1 and S_2 being grounded but phase biased. A first result is that the energy and phase symmetries of the Andreev reflection probability are broken above the gap. Second, the Tomasch conductance oscillations become phase sensitive and they are amplified. Third, the subgap conductance displays a resonant behavior close to the ABS state energies, yielding an ABS spectroscopy tool. Changing the interface parameters, this resonance crosses over between a conductance maximum, featuring "transmission" tunneling spectroscopy, and a conductance minimum, featuring "reflection" spectroscopy. The first situation is encountered when the NIS_1 barrier is a tunnel barrier or at least less transparent than the S_1IS_2 one, while the second case, less conventional, corresponds to the converse where the NIS_1 barrier is more transparent than the S_1IS_2 one. The perfect cancellation of the conductance at $\varphi = \pi$ at the ABS energy is a striking property, due to the suppression of the Andreev reflection by interference between the two interfaces.

Section II presents the model and an analytical solution for the simple limiting case of perfectly transparent interfaces. Section III focuses on the conductance above the gap. Section IV details the subgap conductance. Section V provides a general discussion.

II. THE MODEL

A. Matching equations

A double NIS_1IS_2 interface is considered. For the sake of simplicity, we assume that the Fermi energy and velocity are the same in all materials and that the superconductors S_1 and S_2 have the same gaps (this corresponds to the scheme of Fig. 1, where the superconducting loop is made of the same material). The barrier transparencies are defined as $Z_{1,2} = H_1/\hbar v_F$ where $H_{1,2}$ are the amplitudes of δ-function barriers at the interfaces [6]. The phases are $\varphi_1 = 0$ and $\varphi_2 = \varphi$. This one-dimensional model can be extended to more realistic interfaces, as discussed at the end of the paper. In the case of N and S having different electronic parameters, this is known to quantitatively modify the scattering equations, making the NS_1 barrier less transparent. For instance, for a transparent interface, a wave-vector mismatch $k_F/k_S \neq 1$ is exactly equivalent to an effective barrier Z_{eff}. The main conclusions of the work will thus not be qualitatively modified, and the present calculation can be easily extended to take into account a parameter mismatch. Following Ref. [6] (BTK), a right-moving electron wave function in N is incoming onto the interface. The quasiparticle wave functions in N, S_1, and S_2 can then be written as

$$\begin{aligned}
\Psi^e_N(x) &= \begin{pmatrix}1\\0\end{pmatrix}(e^{iq^+x} + b\,e^{-iq^+x}) + \begin{pmatrix}0\\1\end{pmatrix} a\,e^{iq^-x},\\
\Psi^e_{S_1}(x) &= \begin{pmatrix}u_0\\v_0\end{pmatrix}(\alpha_n\,e^{ik^+x} + \beta_n\,e^{-ik^+x})\\
&\quad + \begin{pmatrix}v_0\\u_0\end{pmatrix}(\alpha_a\,e^{ik^-x} + \beta_a\,e^{-ik^-x}),\\
\Psi^e_{S_2}(x) &= \begin{pmatrix}u_0e^{i\varphi}\\v_0\end{pmatrix} c\,e^{ik^+x} + \begin{pmatrix}v_0e^{i\varphi}\\u_0\end{pmatrix} d\,e^{-ik^-x},
\end{aligned} \tag{1}$$

where a, b, α_n, β_n, α_a, β_a, c, d are amplitude probabilities: a (b) for Andreev (normal) reflection to the left in N, α_n (β_a) for electronlike (holelike) right-moving waves in S_1, β_n (α_a) for electronlike (holelike) left-moving waves in S_1, c (d) for electronlike (holelike) right-moving waves in S_2 (see Fig. 2). Here

$$\begin{aligned}
\hbar q^\pm &= \sqrt{2m(\mu \pm E)}, \quad \hbar k^\pm = \sqrt{2m}[\mu \pm \sqrt{E^2-\Delta^2}]^{1/2},\\
u_0^2 &= \frac{1}{2}\left(1 + \frac{\sqrt{E^2-\Delta^2}}{E}\right) = 1 - v_0^2,
\end{aligned} \tag{2}$$

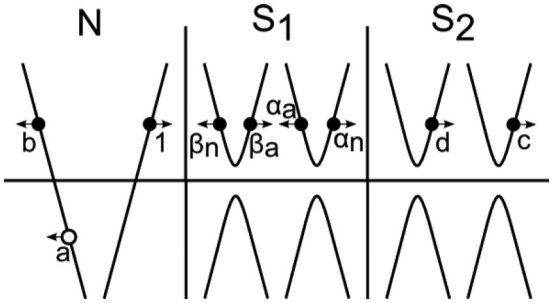

FIG. 2. Semiconductor diagram for an incident electron at the double NIS_1IS_2 interface.

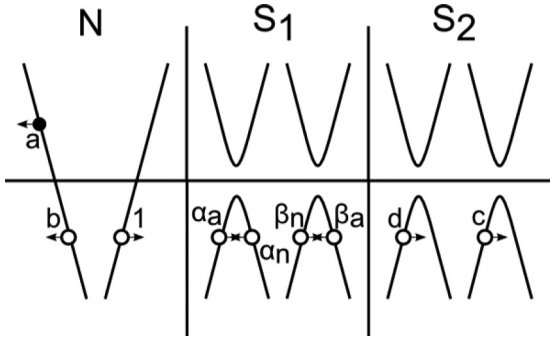

FIG. 3. Semiconductor diagram for an incident hole at the double NIS_1IS_2 interface. The amplitudes $a,b,\ldots$ are related to those of Fig. 2 by symmetry.

with the relation $u_0(-E) = v_0(E)$ and $v_0(-E) = -u_0(E)$. As shown below, generically, here for a nonzero phase difference, the conductance is *not symmetric* in energy, e.g., the standard BTK relation $A(E) = A(-E)$ for a single interface does not hold any longer in the considered setup (see Table I). It is therefore convenient to use Eq. (1) for $E > 0$, and to use instead for $E < 0$ similar equations for an incoming hole with amplitudes $\bar{a},\bar{b}$, etc. (see Fig. 3),

$$\begin{aligned}
\Psi^h_N(x) &= \begin{pmatrix}0\\1\end{pmatrix}(e^{-iq^-x} + \bar{b}\,e^{iq^-x}) + \begin{pmatrix}1\\0\end{pmatrix}\bar{a}\,e^{-iq^+x},\\
\Psi^h_{S_1}(x) &= \begin{pmatrix}u_0\\v_0\end{pmatrix}(\bar{\alpha}_n\,e^{ik^-x} + \bar{\beta}_n\,e^{-ik^-x})\\
&\quad + \begin{pmatrix}v_0\\u_0\end{pmatrix}(\bar{\alpha}_a\,e^{ik^+x} + \bar{\beta}_a\,e^{-ik^+x}),\\
\Psi^h_{S_2}(x) &= \begin{pmatrix}u_0e^{i\varphi}\\v_0\end{pmatrix}\bar{c}\,e^{-ik^-x} + \begin{pmatrix}v_0e^{i\varphi}\\u_0\end{pmatrix}\bar{d}\,e^{ik^+x}.
\end{aligned} \tag{3}$$

Denoting as $B^{ee}(E) = b(E)b^*(E)$ and $A^{eh}(E) = \bar{a}(E)\bar{a}^*(E)$ the normally reflected probability and the Andreev reflected one, respectively (from a hole at energy E to an electron at energy $-E$), the quasiparticle current entering S_1 is given by [6]

$$\begin{aligned}
I = 2N(0)ev_F\mathcal{A}\int_{-\infty}^{\infty}&[f_0(E-eV) - f_0(E)]\\
&\times [1 + A^{eh}(E) - B^{ee}(E)]dE,
\end{aligned} \tag{4}$$

where $N(0)$ is the Fermi density of states in N, v_F the Fermi velocity, and $\mathcal{A}$ the junction area. $f_0(E)$ is the equilibrium Fermi distribution. Thus, the differential conductance is at zero temperature [$\mathcal{N} = N(0)v_F\mathcal{A}$ is the number of channels]:

$$G(E) = \frac{dI}{dV} = \frac{2e^2\mathcal{N}}{h}[1 + A^{eh}(E) - B^{ee}(E)]. \tag{5}$$

The reference chemical potential is the one of $S_{1,2}$. The solutions to Eqs. (1) and (3) are obtained by matching the wave function and its derivative at the interface in a standard procedure [6]. Following the Andreev approximation, the wave vectors $k^+ \approx k^- \approx q^+ \approx q^- \approx k_F$ as factors in the derivatives of the wave functions, but their full expressions are kept in the exponentials. A complete analytical solution can be obtained, but it is too lengthy to be reported here. Yet it can be used to check certain symmetry properties. For instance, the time-reversal symmetry is obeyed, manifesting here in the relation $A^{eh}(E,\varphi,k^{+,-}) = A^{he}(-E,-\varphi,-k^{+,-})$ and $B^{ee}(E,\varphi,k^{+,-}) = B^{ee}(E,-\varphi,-k^{+,-})$. The sign change in the phase reflects that of the (orbital) magnetic field, and time symmetry also inverts momenta, as apparent from the matching equations (1) and (3).

B. Analytical results in limiting cases

An analytical solution can be written for perfectly transparent contacts ($Z_1 = Z_2 = 0$). Such perfect contacts are an ideal limiting regime that can be approached with quantum point contacts. For an incoming electron, the solution reads

$$a = \frac{v}{u}\frac{u^2(e^{i\varphi}-1) - (u^2e^{i\varphi} - v^2)e^{-i\kappa L}}{v^2(e^{i\varphi}-1) - (u^2e^{i\varphi} - v^2)e^{-i\kappa L}}, \tag{6}$$

$$c = \frac{1}{u}\frac{(v^2-u^2)e^{-i\kappa L}}{v^2(e^{i\varphi}-1) - (u^2e^{i\varphi} - v^2)e^{-i\kappa L}}, \tag{7}$$

and $b = d = 0$, where $\kappa = k^+ - k^- = \frac{k_F}{\mu}\sqrt{E^2 - \Delta^2}$.

For energies larger than Δ, $e^{-i\kappa L}$ is, in general, a complex number, whereas for energies lower than Δ, $e^{-i\kappa L}$ is always a real number. One verifies easily that $A(E) = 1$ for $E < \Delta$, a result thus insensitive to φ (see Fig. 4).

TABLE I. Summary of the different symmetries for the conductance.

	Figure No.	$(E \to -E)$	$(\varphi \to -\varphi)$	$(E,\varphi) \to (-E,-\varphi)$
Z_1 or $Z_2 = 0$, $E < \Delta$	4, 5, 7(a)	Yes	Yes	Yes
Z_1 or $Z_2 = 0$, $E > \Delta$	4, 5, 7(a)	No	No	Yes
Z_1 and $Z_2 \neq 0$, $E < \Delta$	6, 7(b)	Yes	Yes	Yes
Z_1 and $Z_2 \neq 0$, $E > \Delta$	6, 7(b)	No	No	No

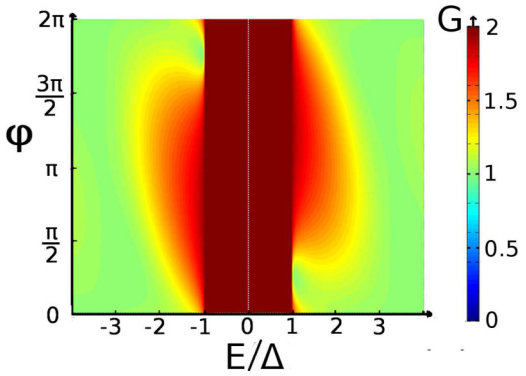

FIG. 4. (Color online) Map of the conductance $G(E,\varphi)$. Case of fully transparent interfaces, $Z_1 = Z_2 = 0$, $L/\xi = 1$. $\Delta/\mu = 0.002$, as in all other figures. No phase sensitivity is obtained below the gap. A phase-sensitive conductance enhancement is obtained above the gap, with a symmetry in the transformation $(E,\varphi \to -E,-\varphi)$.

The situation is different for $E > \Delta$. The condition $\kappa L = 2n\pi$ expresses the occurrence of constructive interferences between the two waves k^+ and k^- within the width of S_1. This leads to the BTK-like scattering amplitudes $a = \frac{v}{u}e^{-i\varphi}, c = \frac{1}{u}e^{-i\varphi}, b = d = 0$.

The condition $\kappa L = 2n\pi$ reads

$$E^2 = \Delta^2 + \frac{4n^2\pi^2\mu^2}{L^2k_F^2}, \tag{8}$$

which indicates the maxima in the Tomasch oscillations.

Another interesting limiting case is that of high energies $E \gg \Delta$, with $u^2 \simeq 1$ and $v^2 \simeq 0$. Then

$$a \simeq \frac{v}{u}[(e^{-i\varphi} - 1)e^{i\kappa L} + 1]; \tag{9}$$

thus,

$$A \simeq \left|\frac{v}{u}\right|^2 [3 - 2\cos(\varphi) - 2\cos(\kappa L) + 2\cos(\varphi - \kappa L)]. \tag{10}$$

Equation (10) leads to $A(\varphi = \pi,\kappa L)/A(\varphi = 0,\kappa L)$ proportional to $5 - 4\cos(\kappa L) \geqslant 1$ for all κL. Thus, the conductance at $\varphi = \pi$ is larger than the conductance at $\varphi = 0$ if $E \gg \Delta$. (see Fig. 4). This trend helps to understand the more general results presented later on.

On the other hand, in the case of an incoming hole, one finds that

$$\bar{a} = \frac{u}{v}\frac{v^2(e^{i\varphi} - 1) - (u^2e^{i\varphi} - v^2)e^{-i\kappa L}}{u^2(e^{i\varphi} - 1) - (u^2e^{i\varphi} - v^2)e^{-i\kappa L}}, \tag{11}$$

$$\bar{c} = \frac{1}{v}\frac{(v^2 - u^2)e^{-i\kappa L}}{u^2(e^{i\varphi} - 1) - (u^2e^{i\varphi} - v^2)e^{-i\kappa L}}, \tag{12}$$

and $\bar{b} = \bar{d} = 0$. Then the question of changing sign of both (E,φ) arises. Indeed, if one changes $u \to v$, $v \to -u$, and $\varphi \to -\varphi$ in Eqs. (6) and (7), one finds that the moduli of a and c in Eqs. (6) and (7), and of $\bar{a}$ and $\bar{c}$ in Eqs. (11) and (12) are respectively equal. There is no symmetry under inversion of E or φ separately, but there is symmetry under simultaneous inversion of (E,φ) (see Fig. 4). As shown below, this does not hold any longer if Z_1 and Z_2 are both nonzero.

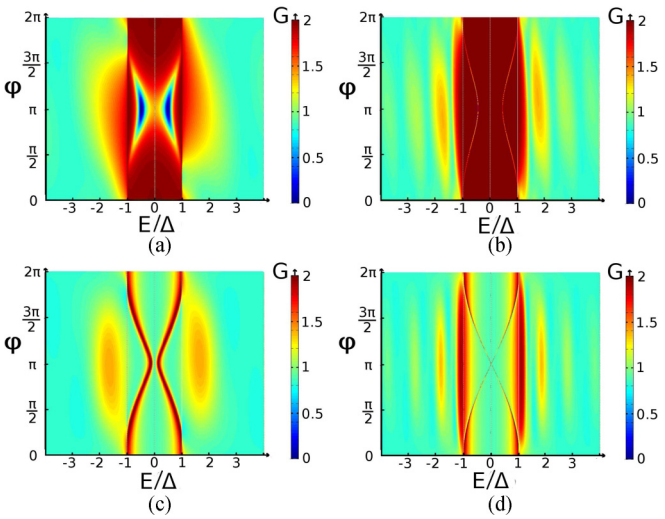

FIG. 5. (Color online) One interface only is transparent. Phase and energy symmetry is obtained below the gap, and phase-sensitive Tomasch oscillations above the gap, being symmetric in the transformation $(E,\varphi \to -E,-\varphi)$. (a) $Z_1 = 0$, $Z_2 = 0.5$, $L/\xi = 1$; (b) $Z_1 = 0$, $Z_2 = 0.5$, $L/\xi = 3$; (c) $Z_1 = 0.5$, $Z_2 = 0$, $L/\xi = 1$; (d) $Z_1 = 0.5$, $Z_2 = 0$, $L/\xi = 3$. In (b), (d), the conductance anomaly at the gap edge is shifted by the phase towards $E > \Delta$, and the Tomasch oscillations are amplified.

III. CONDUCTANCE ABOVE THE GAP

Let us first discuss how the excess conductance due to Andreev reflections above the gap is modified by the phase difference φ. As shown above for perfectly transparent interfaces, the conductance at $\varphi = \pi$ can be much larger than at $\varphi = 0$. This behavior holds also for arbitrary Z_1, Z_2, as seen from the forthcoming discussion.

First, taking either $(Z_1 = 0, Z_2 \neq 0)$ or $(Z_1 \neq 0, Z_2 = 0)$, Fig. 5 shows maps of the conductance as a function of energy E and phase φ for several values of L/ξ. Symmetry of the conductance between (E,φ) and $(-E,-\varphi)$ is obtained in each case. Second, the distinguishing features of Tomasch interferences appear as fringes in Fig. 5. Their enhancement by a phase difference is visible and culminates at $\varphi = \pi$. Moreover, the conductance just above the gap is markedly modified by the phase φ: The gap edge anomaly is shifted to higher energies, with a maximum for $\varphi = \pi$, instead of a gap edge anomaly exactly at $E = \Delta$ for a single NS interface [6].

If none of the barriers is perfectly transparent, e.g., generically $Z_1 \neq 0$ and $Z_2 \neq 0$, then no symmetry exists in energy and phase [see Figs. 6(a) and 7(b)]. As mentioned above, this is not contradictory with the existence of a time-inversion symmetry, but should be traced back to the combination of several relevant phase shifts: those at the interfaces, related to Z_1 and Z_2, the wave-vector phase shifts (k^+L,k^-L), and the φ-dependent Andreev phase shifts at each of the two interfaces. Careful examination of the analytical solution of Eqs. (1) and (3) shows that the probabilities A and B are

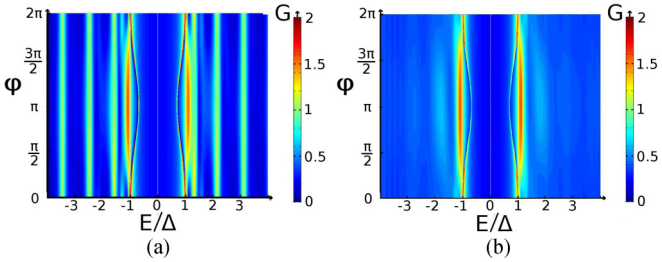

FIG. 6. (Color online) (a) Symmetric barrier case, with $Z_1 = Z_2 = 1, L/\xi = 3$. (b) Same parameters, but averaging L on an interval comparable to ξ.

formed by two kinds of terms. Those involving the phase shift $(k^+ - k^-)L$ happen to be even in Z_1 and Z_2, and they are symmetric in $E,\varphi \to -E,-\varphi$. When Z_1 and Z_2 are both different, new terms containing $(k^+ + k^-)L \sim 2k_F L$ also appear, which are no more even in Z_1 and Z_2, and lead to breaking of the symmetry, e.g., $G(E,\varphi) \neq G(-E,-\varphi)$. This differences oscillates as $\cos 2k_F L$, and is expected to disappear with disorder, interface roughness, or simply two-dimensional character of the interfaces.

On the other hand, when Z_1 and Z_2 are comparable, the behavior for $|E| \gg \Delta$ features a Fabry-Pérot-like cavity, with quasiperiodic fringes extending at high energy [see Fig. 6(a)]. Since in a real experiment with extended interfaces, the length L is expected to fluctuate at the scale of the Fermi wavelength $\lambda_F = \frac{2\pi}{k_F}$, those fringes are expected to partially average out, as seen on Fig. 6(b).

IV. SUBGAP CONDUCTANCE

A. Small $L \lesssim \xi$ case

The subgap conductance exhibits very interesting structures. First, if $L \lesssim \xi$, and with a transparent NS_1 interface, most of the subgap conductance is suppressed for phases close to π, as for instance for $Z_1 = 0, Z_2 = 0.5$ [see Fig. 7(a)]. This is an interference phenomenon, culminating at $\varphi = \pi$, where the amplitudes of Andreev reflections at S_1 and S_2 are just opposite to each other. For small L/ξ, this destructive interference holds in most of the subgap domain. For $L = \xi$ [see Fig. 5(a)] or larger, it concentrates on a narrow energy interval, a phenomenon that we discuss below.

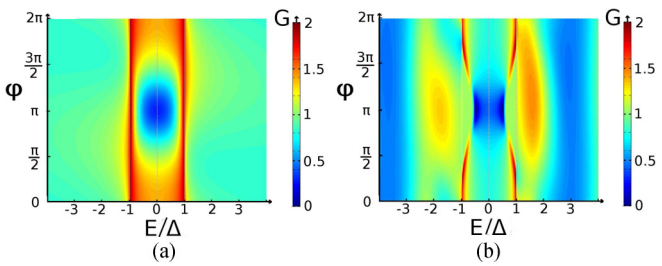

FIG. 7. (Color online) (a) Asymmetric barrier case, with $Z_1 = 0$, $Z_2 = 0.5$, $L/\xi = 0.2$. For a length L shorter than ξ, interferences strongly decrease the subgap conductance. (b) Both nonzero barriers, $Z_1 = 0.5$, $Z_2 = 0.5$, $L/\xi = 1$, no symmetry in energy, and phase is obeyed above the gap for a fixed $k_F L$.

On the other hand, if the first interface is less transparent, for instance $Z_1 = 0.5, Z_2 = 0$, the behavior for $L \lesssim \xi$ displays a pinching of the Andreev resonance anomaly [see Fig. 5(c)], shifted at energies lower than the gap, with a minimum at $\varphi = \pi$, going to zero energy if L is large compared to ξ.

B. Large $L \gtrsim \xi$ case

1. Numerical results

For small Z_1, together with the shift of the Andreev maximum towards above the gap [see Fig. 5(b)], there appears a conductance dip inside the subgap region with high conductance. Conversely, in the opposite case where $Z_1 > Z_2$ [see Fig. 5(d)], the anomaly follows a similar energy and phase variation but is dominated by a conductance excess.

2. Analytical results for the conductance maxima and minima

Those trends are better understood by plotting the subgap conductance as a function of energy, for instance at $\varphi = \pi$ and $L/\xi = 3$. Fixing $Z_2 = 1$ and varying Z_1 from $Z_1 = 0$ to $Z_1 = 2$ shows a drastic evolution (see Fig. 8). For $Z_1 = 0$, a sharp conductance minimum appears, reaching zero. As Z_1 increases, a conductance maximum develops in addition, and it dominates the anomaly for $Z_1 = 2$. The conductance at the minimum is equal to zero only if $\varphi = \pi$. For other values of the phase, the conductance minimum does not reach zero.

An analytical insight of both the minimum and the maximum of the conductance can be obtained. Let us first set $Z_2 = 0$. Then one looks for zeros of the normal reflection coefficient b, meaning that Andreev reflection is total at the NS_1 interface, in spite of $Z_1 \neq 0$. One gets an energy-phase condition

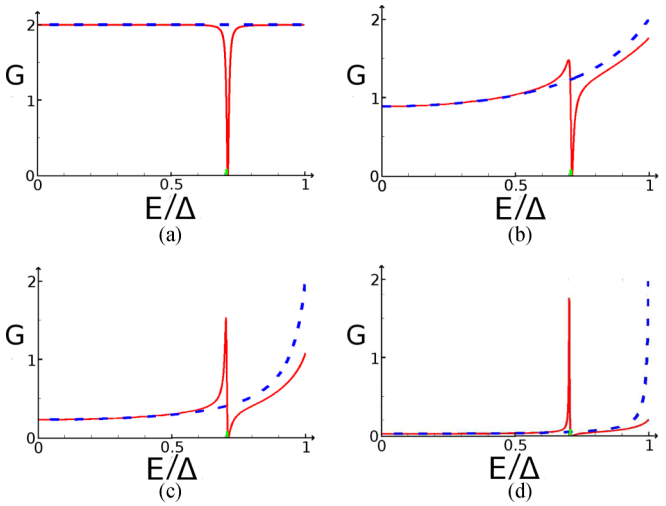

FIG. 8. (Color online) Conductance curve for $Z_2 = 1$, $L/\xi = 3$, $\varphi = \pi$ and different values of Z_1. Red (continuous line): the conductance of the NSS structure. Blue (dotted line): Conductance of the NS junction alone (Z_1 barrier). The zero of G signals the ABS energy for a barrier Z_2. (a) $Z_1 = 0$; (b) $Z_1 = 0.5$; (c) $Z_1 = 1$; (d) $Z_1 = 2$.

(here $x = v_0^2/u_0^2$):

$$\varphi = -i \ln \left\{ \frac{e^{4\kappa L}(x^2+1) - 2x \pm \sqrt{e^{4\kappa L}(x^2-1)[(x^2+1)e^{4\kappa L} - 4x]}}{2x(e^{4\kappa L}-1)} \right\}. \tag{13}$$

If L is large compared to ξ, Eq. (13) simplifies into $\varphi = \mp i \ln(e^{-2i \arccos(E/\Delta)})$, and one obtains

$$E_{\rm ABS} = \pm\Delta \cos\left(\frac{\varphi}{2}\right), \tag{14}$$

corresponding to the ABS energy for a transparent single-channel S_1S_2 contact (or many degenerate channels for a planar interface). If the interface between N and S_1 is not perfectly transparent and if L is large compared to ξ, the normal metal electrode N can act like a side tunneling probe, with a conductance maximum at the the energy of the ABS localized at the S_1S_2 interface [see Figs. 5(d) and 8(d)]. Otherwise, if $L \lesssim \xi$, the barrier at the NS_1 interface perturbs more strongly the reflections involved in the ABS, and an energy gap opens between negative- and positive-energy ABS, as observed in Fig. 5(c), together with substantial broadening.

An unexpected behavior is encountered if the barrier NS_1 is *more* transparent than the Josephson barrier S_1S_2. As shown in Figs. 8(a) and 8(b), the spectroscopic signature of the ABS is a conductance *minimum*. Again, an analytical solution can be obtained for $Z_1 = 0$, looking for maxima (instead of zeros) in the reflection coefficient $b(E)$. This yields

$$e^{i\varphi}\left(Z_2^2+1\right)(x^2+1) - x\left[2e^{i\varphi}\left(Z_2^2+1\right) + (1-e^{i\varphi})^2\right] = 0, \tag{15}$$

where $x = u_0^2/v_0^2$. Solving this equation, one finds

$$E_{\rm ABS} = \pm\Delta\sqrt{1 - T\sin^2(\varphi/2)}, \tag{16}$$

where $T = 1/(1+Z_2^2)$ is the Josephson junction transparency. Equation (16) is the ABS energy for a single channel with barrier Z_2.

V. DISCUSSION AND CONCLUSION

A. Discussion of the results

The above results show that Andreev scattering at a NS_1S_2 interface displays a rich behavior if the width of S_1 is comparable to the coherence length and a phase difference can be applied at the junction S_1S_2. Above the gap, the interferences between quasiparticle modes propagating within S_1 become phase-sensitive, which enhances the Tomasch oscillations with a maximum at $\varphi = \pi$.

An interference occurs between the Andreev scattering amplitudes at the two interfaces for subgap voltage. At large L/ξ, a sharp resonance appears at the energy of the ABS. To be observable, the transparency of the Josephson junction should be large enough, so that the ABS extends inside the superconducting gap. The structure of this resonance displays a maximum and a minimum of conductance, separated by a small energy difference (see Fig. 8). The relative weight of the maximum and minimum depends on the respective transparencies of the two interfaces. When $Z_1 > Z_2$, it is dominated by an enhanced transmission, in a way similar to tunnel spectroscopy. The normal reflection amplitude has a minimum and the Andreev reflection amplitude a maximum. Conversely, when $Z_1 < Z_2$, a destructive interference occurs in the Andreev channel. For $\varphi = \pi$, this interference completely cancels Andreev reflection; thus the conductance becomes zero, and this is even true for any value of Z_1, Z_2, and L, except for very small values $L \ll \xi$ (see Fig. 8). This spectacular result means that the superconductor becomes opaque to quasiparticles coming from the normal metal. Symmetrically, quasiparticles involved in ABS at the S_1S_2 Josephson junction are completely reflected at the NS_1 interface. For phases different from π, reflection is partial, but a sharp minimum occurs and this is enough to detect the ABS. Let us stress that the larger L, the sharper the resonance, which exists even for $L \gg \xi$. This is is due to the divergence of the effective scattering length at the resonance, in a way similar to the usual Andreev resonance at the gap edge in the case of a single NS interface.

It is possible to interpret the conductance maximum and minimum by diagrams in the corresponding limiting cases. Figure 9(a) show a constructive interference between Andreev reflections at NS_1 and S_1S_2, where multiple Andreev reflections builds the ABS. On the other hand, Fig. 9(b) shows a constructive interference between normal reflections at NS_1 and multiple Andreev reflections at S_1S_2. The perfect reflection at NS_1 implies the formation of a resonant state within the superconductor, which involves a Cooper pair crossing S_1S_2 and a crossed Andreev reflection (e-h line in Fig. 10). This three-body process can also be viewed as an exchange process between a single quasiparticle and one member of a Cooper pair, accompanied by a pair crossing the junction.

The situation $Z_1 \ll Z_2$, where the spectroscopic signature of the Andreev states is a conductance minimum, is especially interesting. Then the quasiparticle current flowing at the NS_1 interface can be larger than the critical current at the S_1S_2 junction. The scattering approach does not ensure conservation

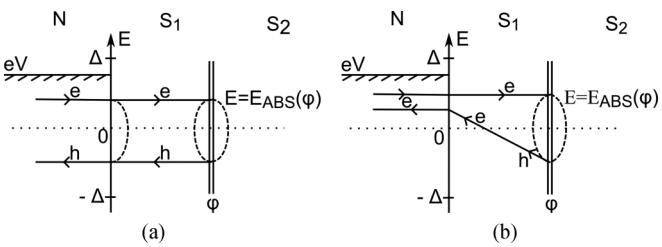

FIG. 9. (a) Scattering diagram showing the cooperative Andreev reflections at the NS_1 interface and at the Josephson S_1S_2 junction, dominating in the large Z_1 case, and responsible for the conductance maximum [Figs. 8(c) and 8(d)]. (b) Scattering diagram showing the normal reflection resulting from the combination of Andreev scattering at S_1S_2 and crossed Andreev process, dominating in the small Z_1 case, and responsible for the conductance minimum of Figs. 8(a) and 8(b).

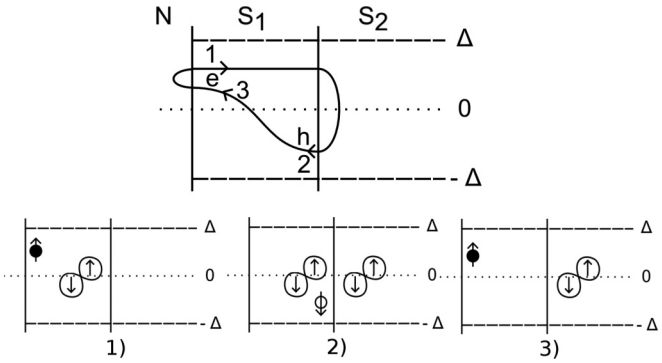

FIG. 10. Diagram showing the resonant state formed with a Cooper pair crossing the S_1S_2 junction and a quasiparticle trapped in S_1 (small Z_1) [Figs. 8(a) and 8(b)]. Steps 1–3 achieve exchange between a single quasiparticle and a Cooper pair crossing the junction. First, an electron (in black) at the NS_1 interface propagates and is reflected into a hole at S_1S_2, while a Cooper pair is transferred at the junction. Second, the reflected hole propagates back to NS_1 into the original electron, in a crossed Andreev process.

of the quasiparticle current, since quasiparticles are converted into Cooper pairs. The excess current in NS_1 compared to S_1S_2 should flow in the upper branch of the setup (Fig. 1).

B. Multichannel or two-dimensional contacts and effects of disorder

The above analysis considers the most simplified one-dimensional model, at zero temperature. It can describe parallel interfaces with the same number of (nondispersive) channels. Or in the spirit of BTK [6], it can be taken as a phenomenological approach to a few-channel point contact probed by a tunneling tip in its close vicinity (or a Sharvin contact). Yet, the general trends of the considered model should be revealed in a more realistic set-up. First, at nonzero temperature, Fermi broadening of the electronic distribution in N will smear the conductance anomalies reported in this work. Second, a multichannel generalization of the scattering method is possible. If the S_1S_2 junction has many dispersive or diffusive channels, it defines ABSs, extending in energy above some minigap $\delta(\varphi)$, and one expects that the anomaly of the conductance will reveal the phase dependence of this minigap (this also holds if the junction is a diffusive SNS junction). Depending on temperature and ABS level spacing, peaks or dips in the conductance can be resolved or, on the contrary, merge into a shoulder (or trough) extending between $\delta(\varphi)$ and the gap Δ.

Disorder such as point disorder in S or interface roughness is expected to have very different effects, depending on whether the voltage is larger or smaller than the gap. In the former case, disorder in the superconductor can easily blur the Tomasch oscillations, unless the elastic mean-free path is larger than L (clean superconductor). In addition, it is expected to restore the symmetry $G(E,\varphi) = G(-E,-\varphi)$. In the subgap regime, on the contrary, the spectroscopic signatures of the ABS are pinned to the ABS energy and should be quite robust, as suggested by averaging out fluctuations in k_FL in the present calculation. Last but not least, disorder in the normal metal N can amplify the Andreev reflection at low energy and give rise to subgap anomalies, by "reflectionless tunneling." To treat all these effects and perform more realistic calculations, in terms of geometry and disorder, one requires more advanced methods using nonequilibrium Green's functions. Such methods also make it possible to calculate the dependence with V of the Josephson current, not addressed in this work. In the case of large transparency and many channels at the NS_1 interface, one should include self-consistency of the gap, and also possible nonequilibrium effects.

In the case of the three-terminal geometry with different superconductors S_1 and S_2, those might have different gaps $\Delta_1 < \Delta_2$. One expects that the structure of the ABS below the smallest gap is revealed in $G(E,\varphi)$ and that a more complex behavior is obtained between Δ_1 and Δ_2.

On the other hand, on the more classic tunnel spectroscopy case $Z_1 \gg Z_2$, where the probe little perturbs the junction, the present configuration is advantageous in terms of spectroscopy of the ABS. This work suggests a "side spectroscopy" by letting a scanning tunneling tip or narrow contact come at a distance of order ξ from the junction (see Fig. 1).

In conclusion, we have revealed the rich behavior a double NSS interface, when the independent control parameters are a voltage bias and a superconducting phase difference, respectively applied to the two interfaces. Phase-sensitive Tomasch oscillations, together with various spectroscopic probes of the ABS, are predictions that could be tested in a realistic device.

ACKNOWLEDGMENTS

The authors acknowledge support from the Agence Nationale de la Recherche (contract Nanoquartets 12 BS10 007 01). The authors also thank H. Courtois, C. Winkelmann, and B. Douçot for fruitful discussions.

[1] A. F. Andreev, Zh. Eksp. Teor. Fiz. **46**, 1823 (1964) [Sov. Phys. JETP **19**, 1228 (1964)].
[2] P. G. de Gennes and D. Saint-James, Phys. Lett. **4**, 151 (1963).
[3] J. M. Rowell and W. L. McMillan, Phys. Rev. Lett. **16**, 453 (1966); J. M. Rowell, *ibid.* **30**, 167 (1973).
[4] W. J. Tomasch, Phys. Rev. Lett. **15**, 672 (1965); **16**, 16 (1966).
[5] W. L. McMillan and P. W. Anderson, Phys. Rev. Lett. **16**, 85 (1966).
[6] G. E. Blonder, M. Tinkham, and T. M. Klapwijk, Phys. Rev. B **25**, 4515 (1982).
[7] I. O. Kulik, Zh. Eksp. Teor. Fiz. **57**, 1745 (1969) [Sov. Phys. JETP **30**, 944 (1970)].
[8] J-D. Pillet, C. Quay, P. Morfin, C. Bena, A. Levy Yeyati, and P. Joyez, Nat. Phys. **6**, 965 (2010).
[9] E. Scheer, P. Joyez, D. Estève, C. Urbina, and M. H. Devoret, Phys. Rev. Lett. **78**, 3535 (1997).
[10] L. Bretheau, Ç. Ö. Girit, H. Pothier, D. Estève, and C. Urbina, Nature (London) **499**, 312 (2013).
[11] B. Dassonneville, M. Ferrier, S. Guéron, and H. Bouchiat, Phys. Rev. Lett. **110**, 217001 (2013).

[12] M. Meschke, J. T. Peltonen, J. P. Pekola, and F. Giazotto, Phys. Rev. B **84**, 214514 (2011).
[13] C. J. Lambert and A. Martin, J. Phys.: Condens. Matter **6**, L221 (1994); A. F. Morpurgo, B. J. van Wees, T. M. Klapwijk, and G. Borghs, Phys. Rev. Lett. **79**, 4010 (1997); A. F. Morpurgo, T. M. Klapwijk, and B. J. van Wees, Appl. Phys. Lett. **72**, 966 (1998); H. Tolga Ilhan and P. F. Bagwell, Appl. Phys. **84**, 6758 (1998).
[14] J. M. Byers and M. E. Flatté, Phys. Rev. Lett. **74**, 306 (1995); T. Martin, Phys. Lett. A **220**, 137 (1996); G. Deutscher andlabe D. Feinberg, Appl. Phys. Lett. **76**, 487 (2000); D. Beckmann, H. B. Weber, and H. v. Löhneysen, Phys. Rev. Lett. **93**, 197003 (2004); S. Russo, M. Kroug, T. M. Klapwijk, and A. F. Morpurgo, *ibid.* **95**, 027002 (2005); P. Cadden-Zimansky and V. Chandrasekhar, *ibid.* **97**, 237003 (2006).
[15] P. Recher, E. V. Sukhorukov, and D. Loss, Phys. Rev. B **63**, 165314 (2001).
[16] J. C. Cuevas and H. Pothier, Phys. Rev. B **75**, 174513 (2007).
[17] M. Houzet and P. Samuelsson, Phys. Rev. B **82**, 060517 (2010).
[18] A. Freyn, B. Douçot, D. Feinberg, and R. Mélin, Phys. Rev. Lett. **106**, 257005 (2011).
[19] T. Jonckheere, J. Rech, T. Martin, B. Douçot, D. Feinberg, and R. Mélin, Phys. Rev. B **87**, 214501 (2013).
[20] B. Kaviraj, O. Coupiac, H. Courtois, and F. Lefloch, Phys. Rev. Lett. **107**, 077005 (2011).
[21] A. H. Pfeffer, J. E. Duvauchelle, H. Courtois, R. Mélin, D. Feinberg, and F. Lefloch, arXiv:1307.4862.
[22] P. G. N. de Vegvar, T. A. Fulton, W. H. Mallison, and R. E. Miller, Phys. Rev. Lett. **73**, 1416 (1994); H. Pothier, S. Guéron, D. Estève, and M. H. Devoret, *ibid.* **73**, 2488 (1994).
[23] P. F. Bagwell, Phys. Rev. B **46**, 12573 (1992).
[24] A. F. Morpurgo and F. Beltram, Phys. Rev. B **50**, 1325 (1994).